Journal of ELECTRONIC MATERIALS, Vol. 44, No. 10, 2015
DOI: 10.1007/s11664-015-3848-8
© 2015 The Minerals, Metals & Materials Society

Electroactive Phase Induced $Bi_4Ti_3O_{12}$–Poly(Vinylidene Difluoride) Composites with Improved Dielectric Properties

SUMIT BHARDWAJ,[1,4,5] JOGINDER PAUL,[1] SUBHASH CHAND,[2] K.K. RAINA,[3] and RAVI KUMAR[1]

1.—Centre for Materials Science and Engineering, National Institute of Technology, Hamirpur, H.P. 177005, India. 2.—Department of Physics, National Institute of Technology, Hamirpur, H.P. 177005, India. 3.—School of Physics and Materials Science, Thapar University, Patiala, Punjab 147004, India. 4.—Department of Materials and Metallurgical Engineering, PEC University of Technology, Sector-12, Chandigarh 160012, India. 5.—e-mail: sumit.bhardwaj4@gmail.com

Lead-free ceramic–polymer composite films containing $Bi_4Ti_3O_{12}$ (BIT) nanocrystals as the active phase and poly(vinylidene difluoride) as the passive matrix were synthesized by spin coating. The films' structural, morphological, and dielectric properties were systemically investigated by varying the weight fraction of BIT. Formation of electroactive β and γ phases were strongly affected by the presence of BIT nanocrystals. Analysis was performed by Fourier-transform infrared and Raman spectroscopy. Morphological studies confirmed the homogeneous dispersion of BIT particles within the polymer matrix. The composite films had dielectric constants as high as 52.8 and low dielectric loss of 0.1 at 100 Hz when the BIT content was 10 wt.%. We suggest that the enhanced electroactive phase content of the polymer matrix and interfacial polarization may contribute to the improved dielectric performance of these composite films. Dielectric modulus analysis was performed to enable understanding of the dielectric relaxation process. Non-Debye-type relaxation behavior was observed for the composite films at high temperature.

Key words: Composites, polymers, dielectric properties, ceramics

INTRODUCTION

Materials with high dielectric constant and low dielectric loss are of immense importance and have been widely used for a wide range of applications in the electronics industry, for example in ferroelectric random-access memory (FeRAM), high-energy storage devices, sensors, and electromechanical transducers.[1–3] Ferroelectric ceramics have a high dielectric constant but are brittle and have a low dielectric strength. Polymers are easy to process, flexible, require low processing temperatures, and have a high dielectric strength. Much effort has thus been devoted to combining the properties of both materials in diphasic compounds, known as ceramic–polymer composites, which combine the high dielectric constants of ceramics with the ease of processing and high dielectric strength of polymers.[4–7]

The development of polymeric dielectric materials has generated much interest in polymers with the appropriate electroactive properties. Among the few polymers with ferroelectric and piezoelectric properties, poly(vinylidene difluoride) (PVDF) and its copolymers are most important. Poly(vinylidene fluoride) (PVDF), a fluorinated polymorphic polymer, has excellent mechanical, insulation, and film-forming properties with excellent piezoelectric, ferroelectric, and pyroelectric properties. PVDF has been widely used in transducers, actuators, and sensors, because of its exceptional electroactive properties, which mostly depend on its polymorphs. Depending on the configuration of the polymer chain, PVDF occurs as four distinct crystalline polymorphs α, β, γ, and δ. Of these, the α phase, the most stable nonpolar phase, has the conformation

(Received March 4, 2015; accepted May 8, 2015; published online June 10, 2015)

TGTG (T, trans; G, gauche). The β phase of PVDF has a planar all-trans (TTTT) conformation. In the β phase the H and F atoms are attached in the chain in such a way that the dipole moments associated with the two C–H and two C–F bonds are additive, and aligned in the direction perpendicular to the carbon backbone resulting in a greater dipole moment, approximately 8×10^{-30} Cm per unit cell.[8–10] The interesting properties of PVDF, in particular those associated with its use in sensors or actuators, are related to the strong electrical dipole moment of the PVDF monomer unit. Moreover, the γ phase is, similar to the β phase, electrically active. However, because of the presence of a gauche bond every fourth repeat of the C–C bond (T3GT3G′), this effect is weaker than for the β phase. The β and γ phases have attracted researchers' interest because of their valuable piezoelectric and ferroelectric properties,[11] and much research is being conducted in attempts to develop materials with high β and γ phase content. In the past few years, the literature has contained reports of studies in which different strategies have been used to obtain and stabilize the β phase, mainly focusing on the development of specific processing procedures and the inclusion of specific fillers. The piezoelectric β-phase can usually be crystallized by poling at high voltage,[12] melt crystallization at high pressure,[13] or electrospinning.[14] Conversion from the α to the β-phase has also been achieved, by stretching of the films at temperatures below 100°C[15] and by recrystallization from mixed solvents.[16] Recent papers report the ability to induce and stabilize the β-phase in the presence of homogeneously dispersed nanofillers, for example silicates and nanoclays.[17,18] Andrew and Clarke and Martins et al. enhanced the electroactive properties of the β-phase by addition of Ni–Zn ferrites and $CoFe_2O_4$–$NiFe_2O_4$ nanoparticles, respectively.[19,20] More recent studies indicate that the γ phase of PVDF is nucleated in the presence of the organoclays. It has been demonstrated that when the composite samples are subjected to a melt-quenched annealing process the nanocomposites crystallize as a mixture of β and γ crystals.[21,22]

In a similar fashion, incorporation of ceramic fillers has positive effect on the properties of nanocomposites, including interfacial area and the polymer phase, with improvement of the dielectric properties. Polymeric materials with high dielectric constants are important in such electronic components as capacitors, gate dielectrics, memory, and energy-storage devices. One common approach used to improve dielectric properties is to disperse high-dielectric-constant ceramic powders within the polymer matrix. Several ceramic powders, for example $BaTiO_3$, $PbTiO_3$, $Pb(Zr,Ti)O_3$(PZT), $Pb(Mg_{1/3}Nb_{2/3})O_3$–$PbTiO_3$, and $CaCu_3Ti_4O_{12}$ (CCTO) have been used as fillers in many high-performance polymers for a variety of dielectric applications.[4,5,23–25] In most of these composites, however, high concentrations of fillers are required, which degrades mechanical properties and processability. An alternative approach is addition of metallic nanoparticles as fillers to the polymer matrix, to obtain metal–polymer composites with ultrahigh dielectric constants and novel three-phase polymer composite systems.[26–28] In recent years, nanoparticles surface-modified by use of organic molecules have also been used to obtain nanocomposites with high dielectric constants.[29,30] However, most of the ceramic fillers used in polymer composite formulations are lead-based, and lead causes severe environmental pollution and is potentially harmful. Thus, much attention has recently been devoted to production of lead-free materials with high dielectric constants.

Over the last few decades, the bismuth-based lead free compound, $Bi_4Ti_3O_{12}$ (BIT) has attracted much attention and become a major focus of scientific interest. BIT is a layered ferroelectric material with a high dielectric constant and a Curie temperature of 675°C. It has high breakdown strength, a high piezoelectric coefficient, and interesting electro-optic switching behavior.[31,32] BIT has attracted much commercial interest for such potential applications as high-temperature piezoelectric devices, memory storage, and optical displays. In recent years, work on bismuth-based polymer composites has focused on the dielectric, optical, and magnetocapacitance behavior of polymer composites.[33–37] As far as the authors are aware, no significant work has been conducted on the effect of dispersion of ferroelectric BIT particles on electroactive phase formation and the dielectric properties of PVDF, which are crucially important if the material is to be used in sensor and FeRAM devices. Homogeneous dispersion of BIT particles may enhance the structural and dielectric properties of PVDF, possibly leading to a new class of lead-free ferroelectric composites for a variety of technological applications.

In this work, processing of BIT–PVDF composite films is addressed. Our composites establish the possibility of nucleating the electroactive phases of PVDF containing dispersions of ceramic particles. It has also been shown that it is possible to prepare BIT–PVDF composites containing the β and γ phases without organic treatment and with low consumption of material. Moreover, the material has a high dielectric constant and a low dissipation factor. Finally, dielectric modulus calculations were conducted to enable understanding of relaxation behavior.

EXPERIMENTAL

Materials

PVDF pellets (M_w = 180,000) used for synthesis of polymer composites were supplied by Sigma–Aldrich. Bi_2O_3 and TiO_2 procured from Sigma–Aldrich (purity 99.9%) were used, without further treatment, as precursors for synthesis of filler particles. Tetrahydrofuran (THF) from Qualigens Fine Chemicals

and *N*,*N*-dimethylformamide (DMF) from Fisher Scientific were used as solvents for fabrication of composite films.

Synthesis of $Bi_4Ti_3O_{12}$ Nanocrystalline Powders

Mechanical activation of nanocrystalline BIT powder was performed in a high-energy planetary ball mill (Fritsch Pulverisette) at room temperature, as reported elsewhere.[38,39] Bi_2O_3 and TiO_2 were used as precursor materials. Stoichiometric amounts of bismuth titanate were weighed, with 3 wt.% excess of Bi_2O_3, and pre-mixed in an agate mortar by hand. The powder was loaded into cylindrical zirconium jars with zirconium balls. The milling conditions were: ball-to-powder weight ratio 20:1, basic disk rotation speed 350 rpm, and milling time 9 h.

Fabrication of $Bi_4Ti_3O_{12}$–PVDF Composite Films

For synthesis of the polymer composites, PVDF pellets were dissolved in 10 ml 1:1 (*v*/*v*) THF–DMF. The solution was magnetically stirred for 8 h at 60°C. When a clear solution was obtained, different amounts of BIT particles (0, 2, 5, 7, 10 wt.%) were added to the solution. The slurry was again magnetically stirred for 2 h and then ultrasonically agitated for 15 min to ensure homogeneous mixing of the particles and to reduce agglomeration. After sonication, the solution was poured dropwise on indium tin oxide-coated and simple glass substrates and spin coated for 1 min with a rotation speed of 1200 rpm. The prepared films were left for 7 days for complete solvent evaporation. The films were annealed in a vacuum oven at 90°C for 5 h. The thickness of the final films was approximately 8 μm.

Characterization Techniques Used

X-ray diffraction (XRD) patterns of BIT ceramic powder and BIT–PVDF composite films were recorded by use of a PANalytical "X"Pert PRO diffractometer with Cu(K_α) radiation (λ = 1.54 Å). Fourier-transform Infrared spectroscopy (FTIR) was performed in the IR region from 400 to 1000 cm^{-1} by use of a Perkin–Elmer model Spectrum-65. Raman spectroscopy was performed by use of a Renishaw Raman microscope. An argon laser of wavelength 514.5 nm operated at 20 mW was used as excitation source. The morphology and approximate size of the BIT particles were investigated by use of a Jeol JEM-2100F transmission electron microscope (TEM) operated at 200 kV. The morphology of the composite films was characterized by field emission scanning electron microscopy (FESEM) with a Quanta FEG-450 with FEI. The thickness of the composite films was measured by use of a Taylor–Hobson Ultra mechanical profiler. Frequency and temperature-dependent dielectric measurements were conducted at room temperature in the frequency range 100 Hz to 1 MHz by use of an Agilent 4284A LCR meter.

RESULTS AND DISCUSSION

Structural Studies

X-ray Diffraction Studies

Figure 1a shows the x-ray diffraction pattern for BIT nanocrystalline powders prepared by high energy ball milling.

All the diffraction peaks were indexed to the single-phase structure of bismuth titanate with an orthorhombic unit cell (JCPDS card no. 89-7500). No impurity peak related to the pyrochlore phase was observed. The lattice constants and unit cell volume were: a = 5.4179 Å, b = 5.4412 Å, c = 32.7987 Å, and V = 966.90 $Å^3$, respectively. The average particle size was determined by use of the Scherrer formula[40]:

$$D = k\lambda/\beta\cos\theta \quad (1)$$

where β is the full width at half maximum (FWHM) for the most intense peak after correcting for peak broadening caused by instrumental error; it was found to be ≈16–18 nm. To determine particle size a TEM image was obtained from bismuth titanate powder milled for 9 h (Fig. 1b). The image revealed that the specimen consisted of nanocrystalline particles and amorphous region of particle size ≈20 nm, in agreement with the XRD study. The particles seemed to have spherical morphology and some aggregations were also observed. Qualitative and quantitative analysis was also performed to confirm the elemental composition of the prepared ceramic particles; the results, shown in Fig. 1c, confirm the formation of single-phase BIT particles. The weight and atomic percentages of the particles are shown in the inset of Fig. 1c.

Figure 2 shows the x-ray diffraction pattern for pure PVDF and BIT–PVDF composite films. For pure PVDF film, the x-ray peak observed at $2\theta \approx 20.8°$ is indicative of the formation of the β-phase (200) and (110) peaks. The small peak at $2\theta \approx 17°$ (denoted *) can be attributed to the α-phase.[41] The more enhanced β-phase in the pure PVDF film can be ascribed to dipolar interaction and hydrogen bonding at the interface between the PVDF nucleus and DMF molecules, which leads to packing of CH_2–CF_2 dipoles in the all-trans conformation.[42] Moreover, on addition of ceramic particles, the small peak at $2\theta \approx 17°$ decreases in intensity then disappears, indicating reduction of the α-phase content of the film. No peak related to the dispersed BIT particles was observed, suggesting that the particles are homogeneously dispersed within the polymer matrix. In addition, no significant change was observed in the x-ray diffraction patterns of composite films. For comparison, the x-ray diffraction pattern of the as-received PVDF pellets used for synthesis of composite films is

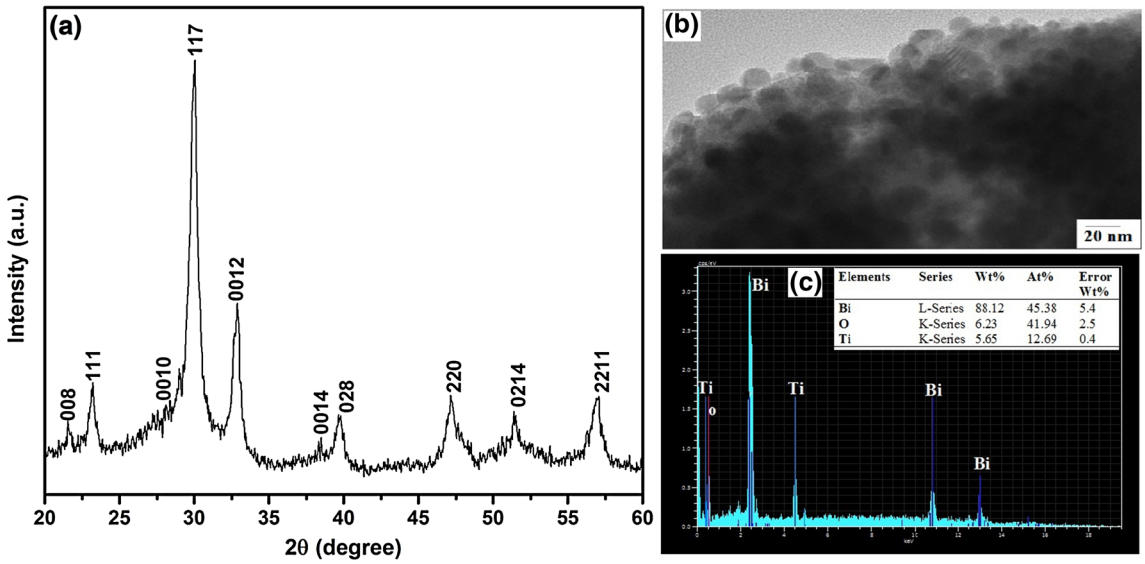

Fig. 1. (a) X-ray diffraction pattern (b) TEM image, and (c) EDS analysis of BIT nanoparticles prepared by high-energy ball milling.

also shown in Fig. 2. The observed (020) and (111) peaks corresponds to the α-phase. Many of these α-phase peaks are suppressed in the diffraction pattern of the spin coated PVDF film, which is a clear indication of a change in the crystal structure of the polymer phase.

FTIR Studies

The FTIR spectrum gives the valuable information about the different crystalline forms of PVDF. Some peaks are unique to each phase and can be used to quantify the amount of phase transformation. The paraelectric α-phase is readily detected and has absorption bands at 489 cm^{-1}, 614 cm^{-1}, 766 cm^{-1}, 795 cm^{-1}, 855 cm^{-1}, and 976 cm^{-1}. However, because of the similar chain conformation of the β and γ phases, distinguishing between these phases is difficult. More precisely, the absorption bands at 510 (CF_2 bending), 840 (CH_2 rocking), and 1276 cm^{-1} (trans band) are characteristic of the β-phase whereas the absorption bands at 431 cm^{-1}, 812 cm^{-1}, 883 cm^{-1}, and 1234 cm^{-1} are characteristic of the γ-phase.[43,44]

FTIR results are commonly used to quantify the electroactive phase content of PVDF. To determine the fraction of the β phase, IR absorption bands at 766 cm^{-1} and 840 cm^{-1}, characteristic of the α and β phases, respectively, and a procedure similar to that of Gregorio and Cestari were used.[45] Assuming IR absorption follows the Lambert–Beer law, the absorbances $A\alpha$ and A_β at 766 cm^{-1} and 840 cm^{-1}, respectively, are given by:

$$A_\alpha = \log \frac{I_\alpha^0}{I_\alpha} = K_\alpha C X_\alpha L \qquad (2)$$

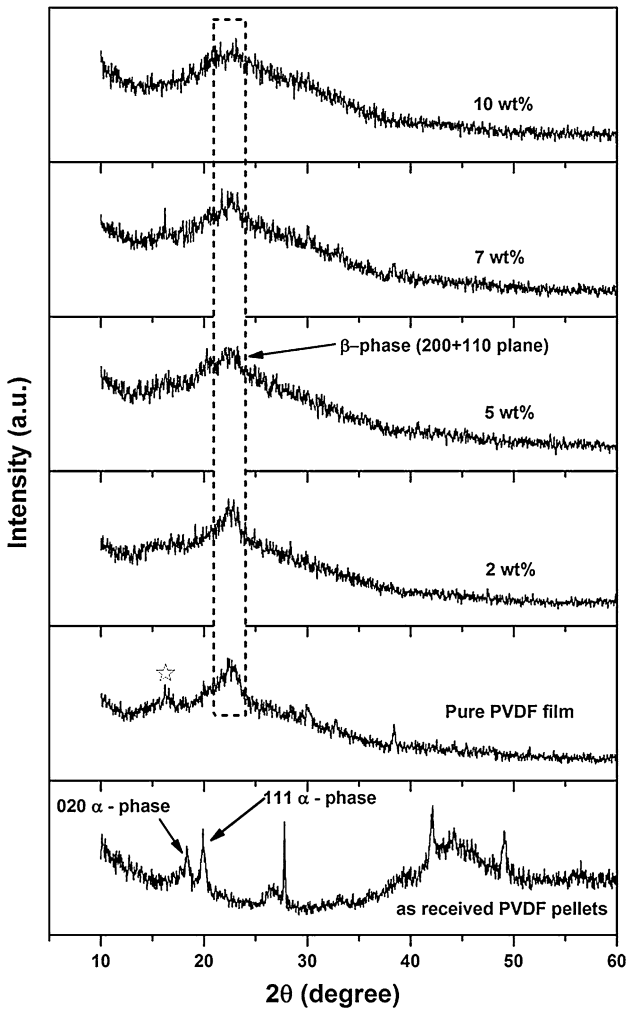

Fig. 2. XRD patterns of pure PVDF and BIT–PVDF composite films.

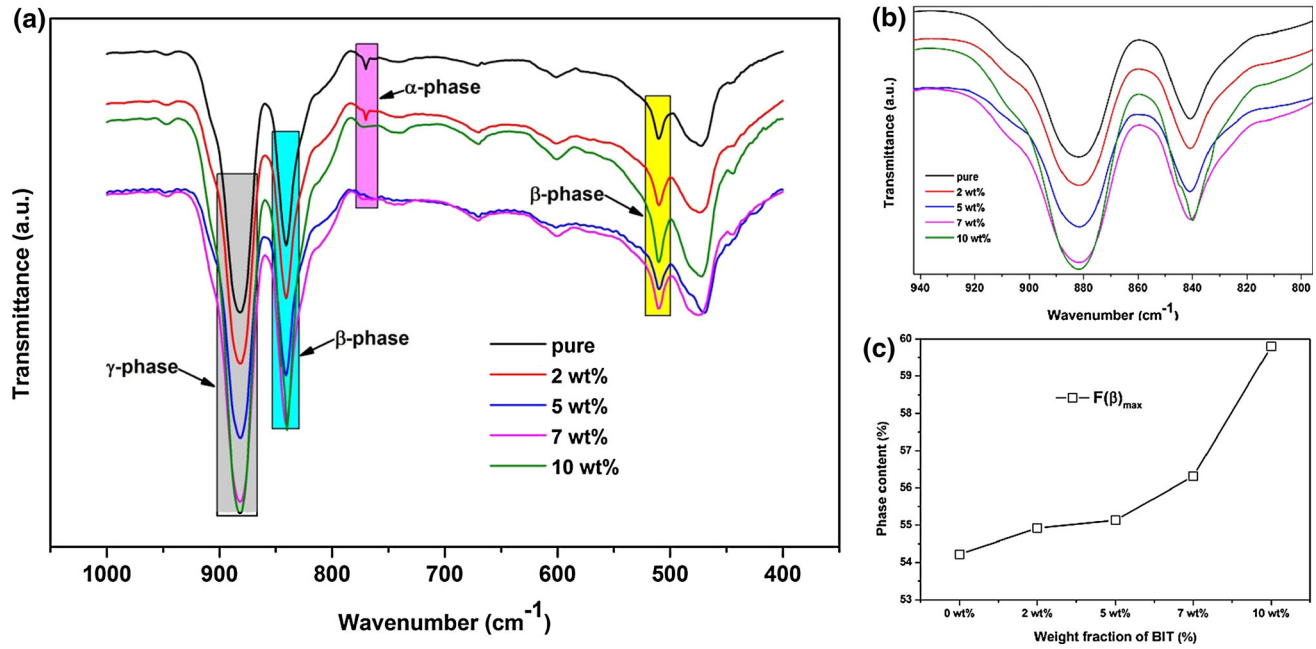

Fig. 3. (a) FTIR spectra of pure PVDF and BIT–PVDF composite films. (b) Enlarged view of the FTIR peaks at 840 cm^{-1} and 883 cm^{-1}. (c) Variation of the maximum content of β phase, $F(\beta_{max})$, as a function of wt.% BIT.

Table I. Maximum content of the β-phase, $F(\beta_{max})$, dielectric constant, and dielectric loss for pure PVDF and BIT–PVDF composite films

BIT wt.%	$F(\beta)_{max}$	Dielectric constant	Dielectric loss
Pure	54.2	19.7	0.014
2 wt.%	54.9	27.9	0.009
5 wt.%	55.1	30.8	0.082
7 wt.%	56.3	45.4	0.085
10 wt.%	59.8	52.7	0.1

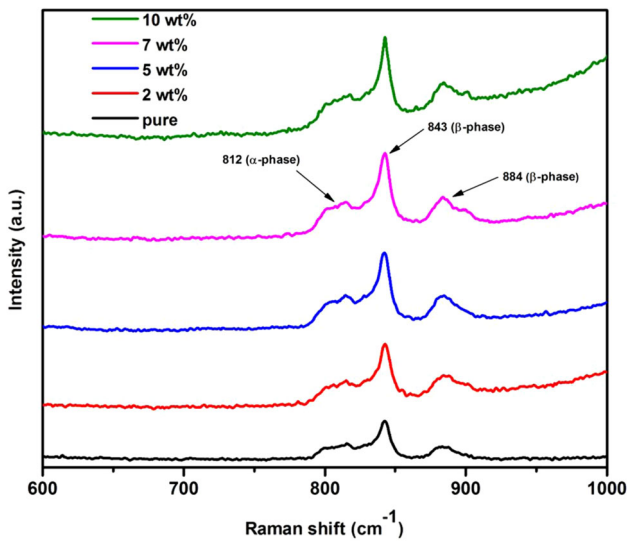

Fig. 4. Raman spectra of pure PVDF and BIT–PVDF composite films.

$$A_\beta = \log\frac{I_\beta^0}{I_\beta} = K_\beta C X_\beta L \tag{3}$$

where L is the thickness of the sample and C is the average total monomer concentration. $I^0$and I are the intensities of incident and transmitted radiation, respectively. The value of $K\alpha$ is 6.1×10^4 and $K\beta$ is 7.7×10^4 cm^2/mol. For a system containing the α and β phases, the relative fraction of the β phase, $F(\beta)$ can be calculated by use of the formula:

$$F(\beta) = \frac{X_\beta}{X_\alpha + X_\beta} = \frac{A_\beta}{\left(K_\beta/K_\alpha\right)A_\alpha + A_\beta} = \frac{A_\beta}{1.26A_\alpha + A_\beta} \tag{4}$$

FTIR spectra of pure PVDF and of BIT–PVDF composite films containing different amounts of

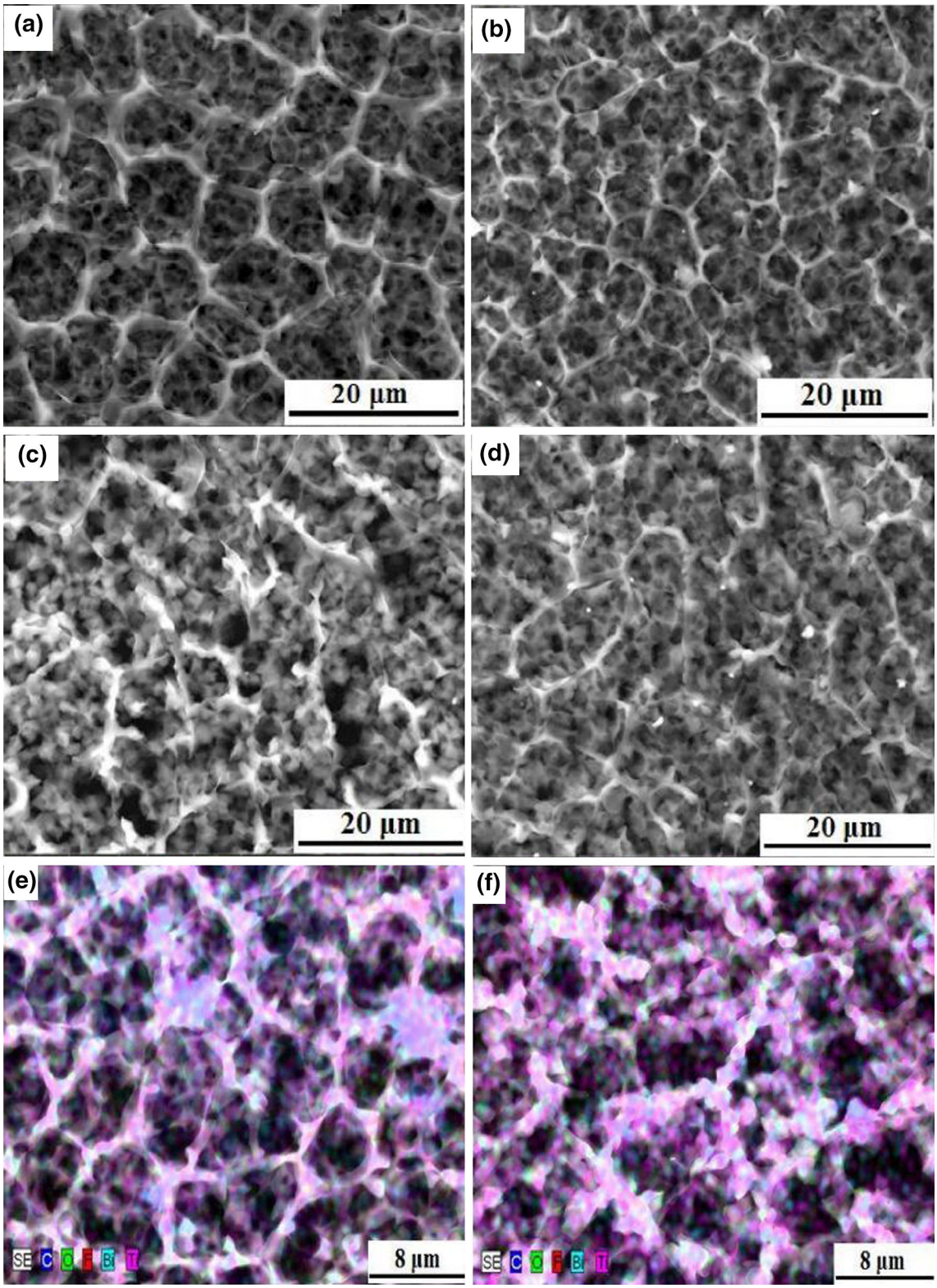

Fig. 5. FE-SEM images of: (a) pure PVDF and (b) 2 wt.%, (c) 5 wt.%, (d) 7 wt.%-loaded BIT–PVDF composite films. Mapping data for (e) 7 wt.% and (f) 10 wt.% BIT–PVDF composite films.

ceramic particles addition are shown in Fig. 3. The strong absorption bands of the β phase at 510 cm^{-1} and 840 cm^{-1} are apparent in each of the spectra, with a strong absorption band characteristic of the γ phase at 883 cm^{-1}. The small amount of the α phase was also apparent from the peak at 766 cm^{-1}. The

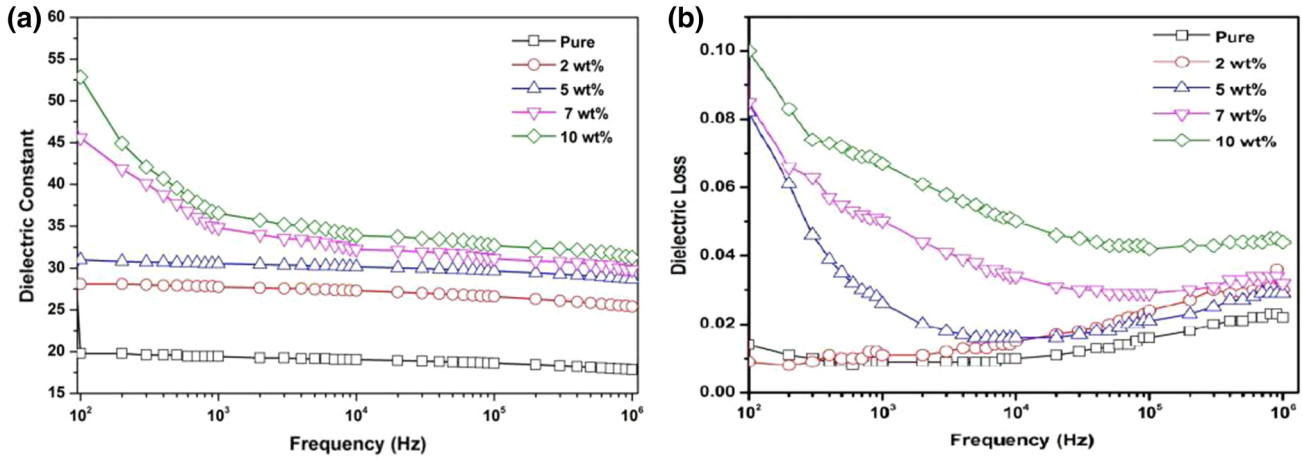

Fig. 6. Frequency dependence of (a) dielectric constant and (b) dielectric loss for pure PVDF and BIT–PVDF composite films, measured at room temperature.

intensities of the peaks from the β (510 cm^{-1} and 840 cm^{-1}) and γ (883 cm^{-1}) phases were greater than those in the spectra from materials with increased particle loading. However, the corresponding absorption band for the α-phase (766 cm^{-1}) diminished and almost disappears at higher particle loading. For more clarity, an enlarged view of absorption bands at 840 cm^{-1} and 883 cm^{-1} is shown in Fig. 3b. Enhancement of peaks from the electroactive β and γ phases indicates that the α-phase is being converted to the more stretched β and γ phases. Quantification of enhancement for the β phase containing ceramic particles was performed by use of Eq. 4. The β phase content was found to increase markedly on increasing the BIT content, as shown in Fig. 3c. Detailed values of $F(\beta_{max})$ for all composite films are listed in Table I. This increase in relative intensity of the β and γ phases and the disappearance of the α-phase is observed only when the particles are well dispersed within the polymer matrix.

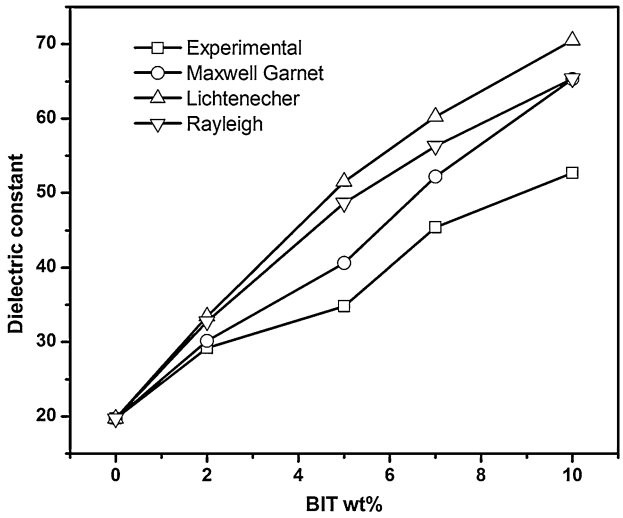

Fig. 7. Experimental and theoretical dielectric constants for BIT–PVDF composites films at 100 Hz and room temperature.

Raman Studies

Raman spectroscopy was performed to confirm the polymorphic changes of the PVDF induced by inclusion of the ceramic particles. Raman spectra provide information about the conjugated structure and chain skeleton of polymers. The wt.%-dependent Raman spectra of BIT–PVDF composite films are shown in Fig. 4. The spectral bands at approximately 843 cm^{-1} and 884 cm^{-1} are attributed to the symmetric CF_2 stretching modes of the electroactive β-phase whereas the small hump at approximately 812 cm^{-1} is associated with the symmetric CF_2 stretching mode of the α-phase.[46] From the spectra it is clearly apparent that the characteristic Raman bands of the β-phase are present in each of the spectra and that the relative intensity of these bands increases with BIT particle loading. However, the corresponding Raman band associated with the α-phase becomes broader with increasing BIT loading.

It is well known that the electroactive β-phase has the highest dipolar moment per unit cell, compared with the other phases. In the β-phase, polymer chains are arranged in pseudo hexagonal lattices, which accounts for the enhanced dielectric and ferroelectric properties of the phase.[11] The enhancement of the electroactive properties of the β and γ phases by inclusion of BIT particles can be explained by different mechanisms.

1. First, it can be explained by the Flory lattice theory introduced by Mackay et al.[47] They included enthalpic effects on polymers of mixing with nanoparticles. They demonstrated that the dispersed nanoparticles cause the polymer to expand, when the radius of the dispersed

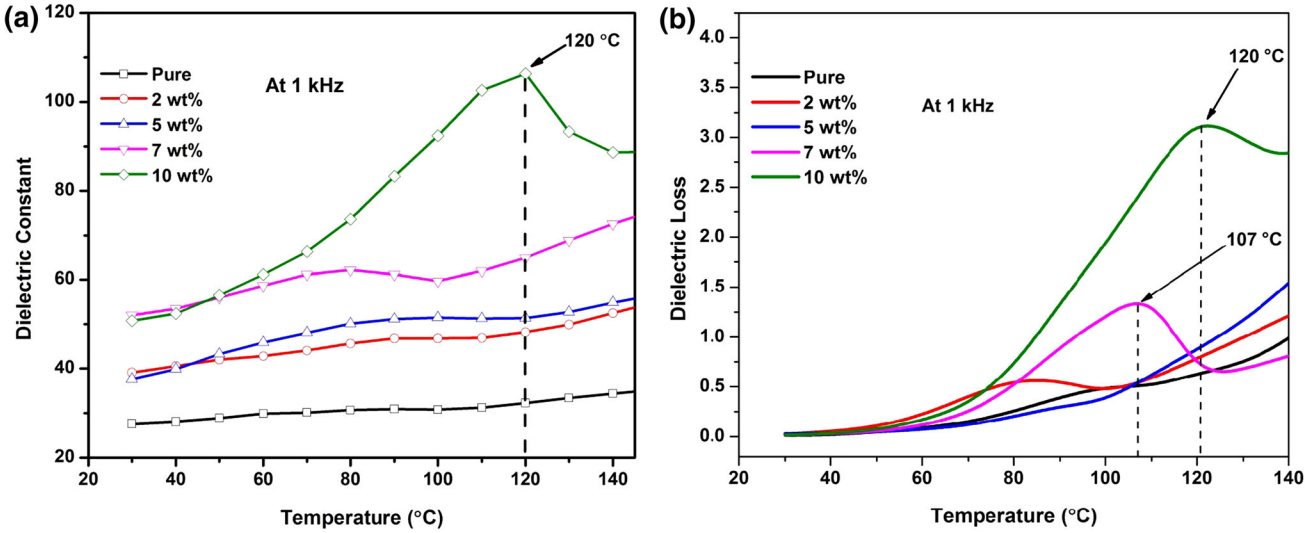

Fig. 8. Temperature dependence of (a) dielectric constant and (b) dielectric loss for pure PVDF and BIT–PVDF composite films.

nanoparticles is less than the radius of gyration (R_g) of the polymer. The R_g value of the PVDF used in this work was 27.5 nm whereas the average diameter of the BIT nanoparticles used was ≈20 nm. i.e. smaller than the R_g values of PVDF.[19] Therefore, as the BIT particles are dispersed in the PVDF matrix, the polymer swells, leading to an increase in its radius of gyration. This increase in the radius of gyration, or expansion of the polymer chains, results in more extended forms of the polymer, i.e. the all -trans β and T3GT3G', γ phases. Therefore, the observed increase in $F(\beta)_{max}$ of the BIT–PVDF composite films can be attributed to the increase in the R_g value of the polymer, which promotes chain ordering into more extended β and γ phases.

2. Second, the nanoparticles used for synthesis of polymer composites contain bismuth ions with two lone pairs of electrons. Nucleation of the electroactive β and γ phases can be regarded as a consequence of the interaction between the lone pairs of electrons and the dipolar moments of PVDF. This interaction tends to align the PVDF monomers in, predominantly, the all-trans conformation, inducing crystallization of β phase.
3. BIT is a well-known ferroelectric material. Homogeneous dispersion of the BIT particles might be interrupting the chain mobility of PVDF, facilitating transformation between the non-polar and polar phases and possibly increasing the number of nucleation sites during the crystallization process. This will further increase the amounts of the electroactive β and γ phases of the polymer.

Hence, XRD, FTIR, and Raman studies support the formation and enhancement of the relative amounts of the electroactive β and γ phases on incorporation of BIT particles. These results are in agreement with previously reported results which reveal increases in the amounts of the electroactive phases of PVDF on incorporation of a variety of different types of nanofiller within the polymer matrix.[19,48,49] Because the β and γ phases are the most electrically active phases, increasing their amounts in BIT–PVDF composite films is an on-going pursuit because of strong interest in such applications as sensors, actuators, batteries, filters, chemical warfare protection, magnetoelectrics, and, more recently, biomedicine.

Study of Morphology

Increased amounts of the β and γ phases is observed only when the ceramic particles are well dispersed within the polymer matrix. FE-SEM measurements were performed to visualize the distribution of the ceramic particles. Figure 5 shows the FESEM images of pure PVDF and its composite films. Pure PVDF film (Fig. 5a) has a typical spherulitic type microstructure in which the polymer chains are self-connected into a continuous network. A similar structure consisting of well-connected spherulites with clear boundaries has been observed in Nylon-6 membranes.[50] Incorporation of the BIT particles has a significant effect on the spherulitic structure of the composite films. Inclusion of the BIT particles will restrict the nucleation process and growth kinetics of the spherulites. For higher BIT wt.% (5 wt.% and 10 wt.%), the filler particles will hinder the growth of spherulites and, therefore, prevent formation of the characteristic spherulitic microstructure of the polymer. It is apparent that the BIT particles are almost uniformly dispersed within the polymer matrix. Figure 4e–f show the mapping data for 7 wt.% and 10 wt.% BIT–PVDF composite films. The mapping data clearly demonstrate the uniform dispersion of the BIT particles within the polymer

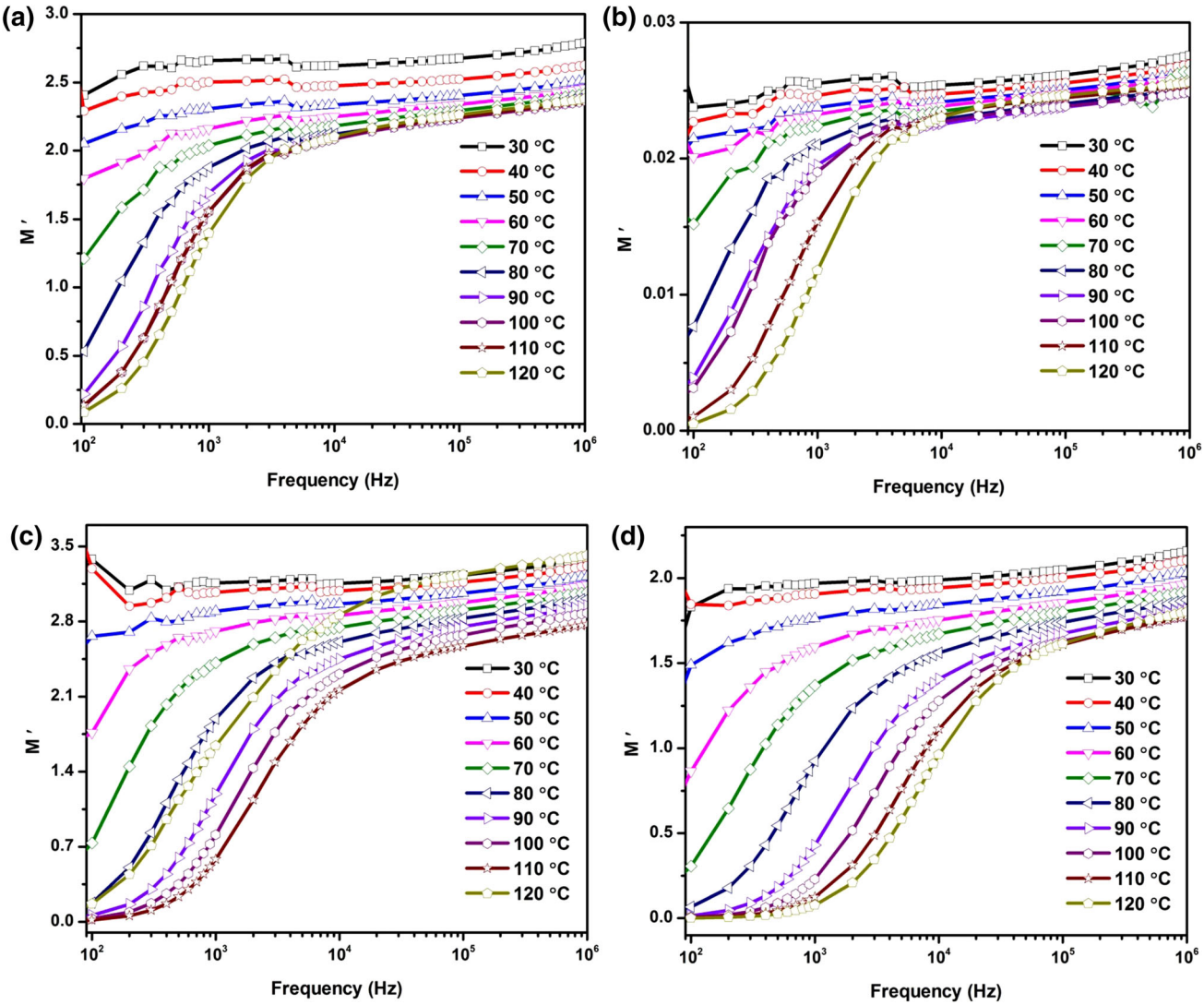

Fig. 9. Variation of the real part of dielectric modulus *M′* as a function of frequency at different temperatures for (a) pure PVDF and (b) 5 wt.%, (c) 7 wt.%, and (d) 10 wt.% BIT–PVDF composite films.

matrix without appreciable agglomeration. Moreover, at higher wt.% BIT inclusion, more interfaces are formed between the BIT particles and the PVDF matrix. Therefore, the microstructure, in conjunction with structural studies, confirms that the BIT particles are well distributed throughout the polymer matrix and increase the nucleation effect of the β phase of polymer. The good dispersion and homogeneous packing of ceramic fillers is likely to result in superior dielectric and ferroelectric properties.

Dielectric Studies

Dependence of Dielectric Constant and Dielectric Loss on Frequency and Composition

Figure 6 shows the frequency dependence of dielectric constant and dielectric loss for pure PVDF and its composite films, in the range 10^2 Hz to 10^6 Hz at room temperature. Figure 6a shows that the relative dielectric constant of the composite films increases linearly with increasing BIT particle loading at 100 Hz, from 19.6 for pristine PVDF film to 52.7 for 10 wt.%-loaded BIT–PVDF composite film. The graph also shows that for lower BIT loading (2 wt.% and 5 wt.%) the stability of the dielectric constant of the composites in this frequency range is good, remaining almost parallel to the frequency axis on the log scale. However, the graph also shows large dependence on frequency for higher particle loading (7 wt.% and 10 wt.%). The dielectric constant decreases rapidly in the lower frequency range 10^2 Hz to 10^4 Hz and then remains constant from 10^4 Hz to 10^6 Hz. This increase in the dielectric constant at 7 and 10 wt.% particle loading can be attributed to the Maxwell–Wagner–Sillars (MWS) polarization effect,[51,52] in which charges are accumulated at the interface between BIT particles

and PVDF because of their different dielectric constants and conductivity. For larger amounts of BIT, more interfacial areas are introduced between the BIT particles and the PVDF matrix. This results in larger interfacial polarization and thus increases in dielectric constants of the composite films. As confirmed by FTIR and Raman studies, the composite films contain a greater proportion of the β phase (i.e. $F(\beta)_{max}$ is greater). The β-phase, in which the polymer chains are arranged in the all-trans configuration, is responsible for its exceptional dielectric and ferroelectric properties. Increasing the electroactive phase content of the composite films may lead to a closer chain packing and greater dipole density. Therefore, the composite films have higher dielectric constants.

Figure 6b shows the variation in dielectric loss for pure PVDF and BIT–PVDF composite films at room temperature. The dielectric loss increases almost linearly with increasing ceramic particle loading, maintaining, nevertheless, values <0.1 even for the highest ceramic particle loadings (10 wt.%), showing that the material has potential application as a dielectric material. It is apparent that the dielectric loss first decreases in the range 10^2–10^4 Hz then subsequently increases with increasing frequency up to 10^6 Hz. In the low frequency range, the relaxation process is attributed to the molecular motion accompanied by the change of dipole moment in the crystalline regions, whereas at high frequencies the relaxation process involves contributions from two types of molecular motion, micro-Brownian motion of amorphous chain segments and molecular motion at the interfaces.[53,54] In the high-frequency range, the relaxation peak of composite films is more intense than that of the pure PVDF film, suggesting that the relaxation peak amplitude is mainly determined by the total area of the

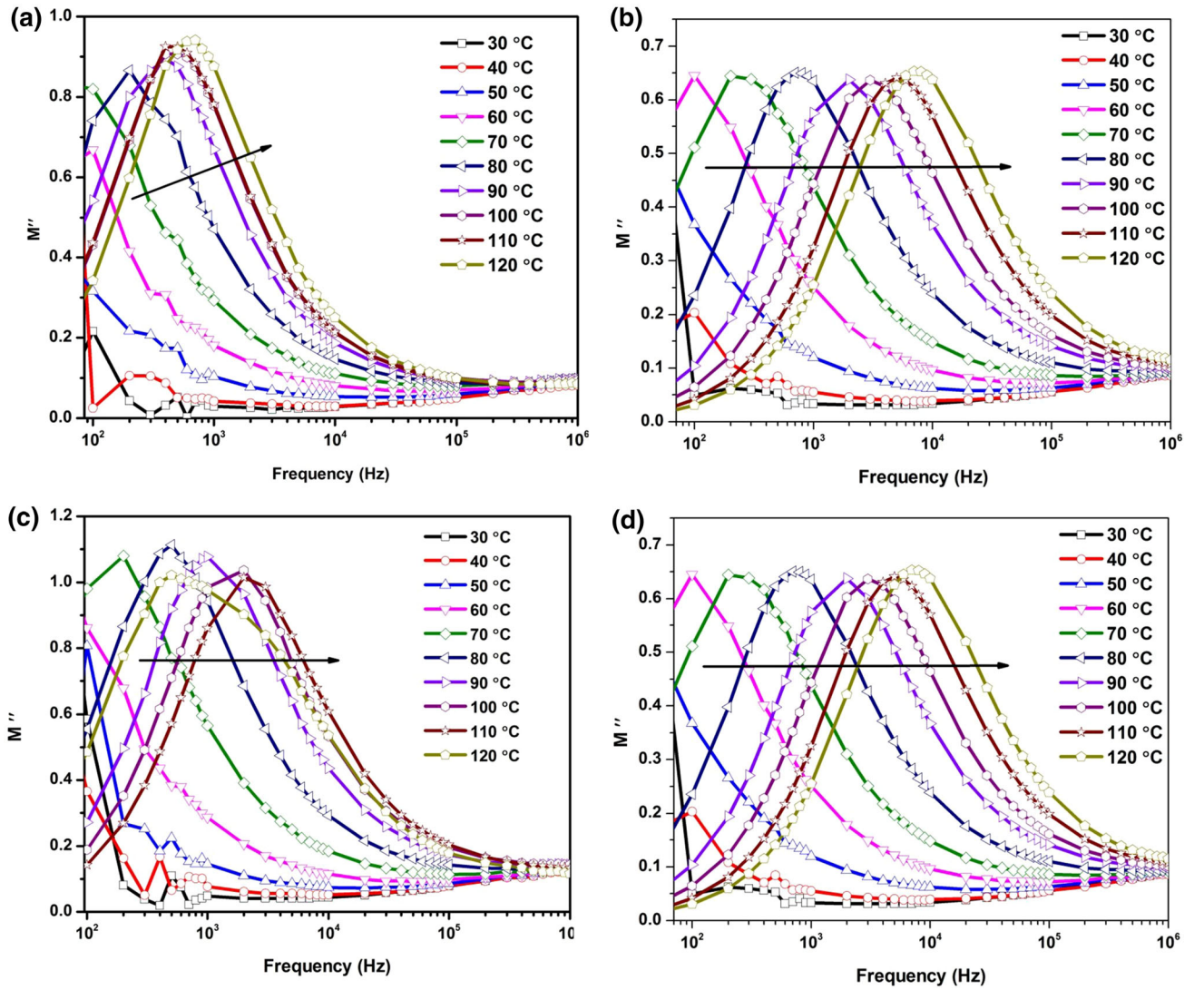

Fig. 10. Variation of the imaginary part of dielectric modulus M'' as a function of frequency at different temperatures for (a) pure PVDF and (b) 5 wt.%, (c) 7 wt.%, and (d) 10 wt.% BIT–PVDF composite films.

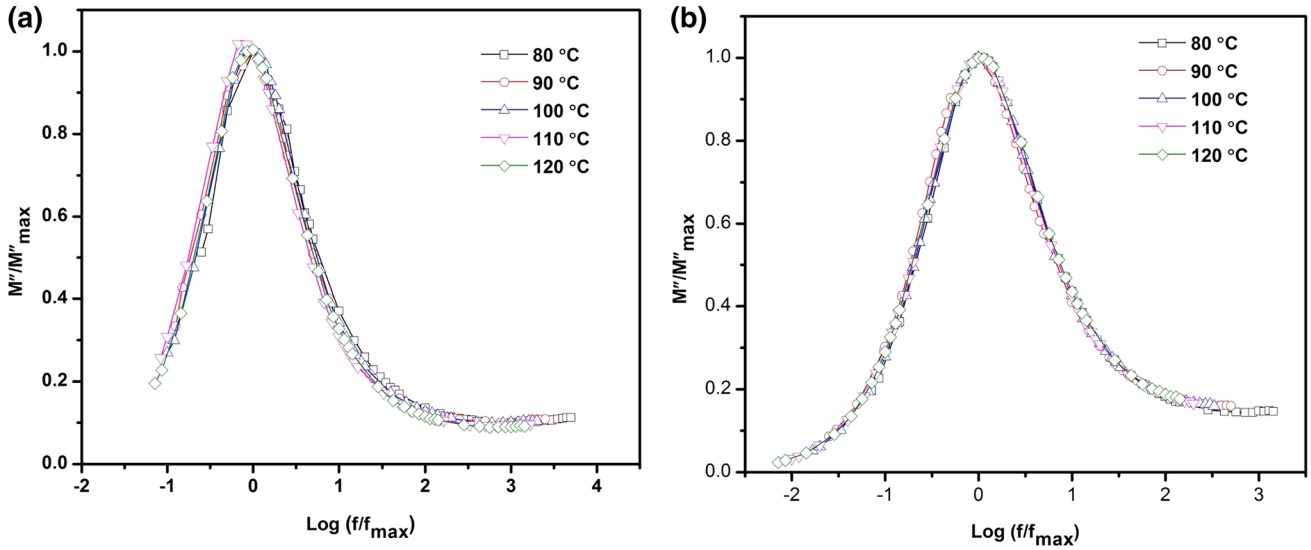

Fig. 11. Master modulus curve for (a) pure PVDF and (b) 10 wt.% BIT–PVDF composite film at different temperatures.

Table II. Maximum peak frequency f_{max}, full width at half maximum (FWHM), β and relaxation time τ at different temperatures for pure PVDF and 10 wt.%-loaded BIT–PVDF composite film

Composition	Pure PVDF film				10 wt.% BIT–PVDF composite film			
Temperature (°C)	f_{max} (Hz)	FWHM	β	$\tau(s)$	f_{max} (Hz)	FWHM	β	$\tau(s)$
80	200	3.24	0.351	7.96×10^{-4}	700	3.17	0.359	2.27×10^{-4}
90	400	3.22	0.353	3.98×10^{-4}	2000	3.14	0.362	7.96×10^{-5}
100	500	3.12	0.364	3.18×10^{-4}	3000	3.30	0.345	5.30×10^{-5}
110	600	3.14	0.362	2.65×10^{-4}	5000	3.31	0.344	3.18×10^{-5}
120	700	3.08	0.369	2.27×10^{-4}	7000	3.32	0.343	2.27×10^{-5}

interfaces. These ceramic–polymer composites with low dielectric loss can be used to form capacitors on organic substrates because of the combination of the processability of polymers and the high dielectric constant of ceramic phase. Detailed values of the dielectric constant and dielectric loss are given in Table I.

Prediction of the dielectric behavior of the composite is very important to its application. Therefore, to understand the observed dielectric behavior of the BIT–PVDF composite films, a series of analytical expressions and numerical simulations have been proposed. In this study three approximation models were used to calculate the effective dielectric constant of the BIT–PVDF composites:[55–57] the Maxwell–Garnet equation,

$$\varepsilon_{\text{eff}} = \frac{(2V_f + 1)\varepsilon_f + 2(1 - V_f)\varepsilon_m}{(1 - V_f)\varepsilon_f + (2 + V_f)\varepsilon_m} \cdot \varepsilon_m \qquad (5)$$

the Lichtenecker equation,

$$\varepsilon_{\text{eff}} = \exp[V_f \ln \varepsilon_f + (1 - V_f) \ln \varepsilon_m] \qquad (6)$$

and the Rayleigh Model

$$\varepsilon_{\text{eff}} = \left[\frac{2\varepsilon_m + \varepsilon_f + 2V_f(\varepsilon_f - \varepsilon_m)}{2\varepsilon_m + \varepsilon_f - V_f(\varepsilon_f - \in_m)}\right] \cdot \varepsilon_m \qquad (7)$$

where ε_{eff}, ε_m and ε_f are the permittivity of the composites, matrix and BIT respectively, V_f is the volume fraction of the BIT nanoparticles. The volume fraction of BIT particles for a given weight fraction was determined from the relation $V_f = w_f/w_f + w_m\left(\rho_f/\rho_m\right)$, where, w_f is the weight fraction and ρ_f the density of the BIT particles, and w_m and ρ_m are, respectively, the weight fraction and density of the PVDF matrix.

Figure 7 shows the effective dielectric constant of BIT–PVDF nanocomposite films for different weight percentages, and the values predicted by the equations above at 100 Hz. It is apparent the Lichtenecker logarithmic equation and the Rayleigh model are unable to describe the experimental data. However, dielectric constants calculated by use of the Maxwell–Garnet model are quite close to the experimental results for ceramic weight fractions less than 5 wt.%, although the results deviate for much for higher

weight percentages. This is because the Maxwell–Garnet model predicts the dielectric properties of the composites at relatively low inclusions. This model does not take into account the effect of particle–particle dipole interactions or their effect on the surrounding medium, which becomes important at higher weight fraction. Moreover, the discrepancy between the experimental and calculated results at high weight percentage may also be attributed to the porosity of the nanocomposite film. When this occurs, the polymer phase is no longer a continuous phase in all directions. Consequently, the porosity effect at high filling ratios should be taken into account in treatment of the effective permittivity.

Temperature Dependence of Dielectric Constant and Dielectric Loss

Figure 8 shows the temperature dependence of dielectric constant and dielectric loss for pure PVDF and BIT–PVDF composite films at 1 kHz. As shown in Fig. 8a, the dielectric constant of pure PVDF film is almost constant over a broad temperature range (25–140°C). For the composite films, however, the dielectric constant is much more temperature-dependent and increases with increasing ceramic content over the whole temperature range. It is apparent that for up to 7 wt.%-loaded composite films no clear phase transition is observed and the dielectric constant increases linearly with increasing temperature. However, a well defined dielectric peak at approximately 120°C was observed for 10 wt.%-loaded BIT–PVDF composite film. This dielectric peak is attributed to the ferroelectric to paraelectric phase transition of the PVDF polymer.[58]

Figure 8b shows the temperature dependence of dielectric loss at 1 kHz for pure PVDF and BIT–PVDF composite films. It is apparent that the dielectric loss increases linearly with increasing temperature for all the composite films. For low ceramic content, no ferroelectric to paraelectric phase transition was observed. However, for 7 wt.% and 10 wt.% BIT–PVDF composite films, a well-defined dielectric loss peak was observed at approximately 100–120°C; this is attributed to the phase transition related to PVDF mentioned above. The dielectric loss may be attributed to loss of energy because of micro-Brownian motion of the dipoles and depends on the internal viscosity of the system. In addition, the dielectric loss peak shifts to higher temperature on inclusion of BIT particles—its position changes from 107°C for 7 wt.% to 120°C for 10 wt.%-loaded BIT–PVDF composite films. This shift in the dielectric loss peak is attributed to the interfacial polarization which results from formation of interface boundaries between BIT and the PVDF matrix and the intrinsic ionic polarization of PVDF matrix.

Dielectric Modulus Studies

Dielectric relaxation is sensitive to the motion of charged species and dipoles of the polymer phase. Study of this motion provides essential information on the ionic transport mechanism. Study of the complex dielectric modulus is very important and enables analysis of dynamic aspects of electrical transport processes in materials. The dielectric modulus M^* corresponds to the relaxation of the electric field in the material when the electric displacement remains constant. Therefore the modulus represents the real dielectric relaxation process. The electric modulus is derived from the inverse of the complex dielectric constant ε^*, as[59]:

$$M^*(\omega) = \frac{1}{\varepsilon^*(\omega)} = M'(\omega) + iM''(\omega) \tag{8}$$

The real (M') and imaginary (M'') parts of the complex dielectric modulus were obtained from $\in'(\omega)$ and $\varepsilon''(\omega)$ values using the relation

$$M'(\omega) = \frac{\varepsilon'(\omega)}{\varepsilon'(\omega)^2 + \varepsilon''(\omega)^2} \text{ and } M''(\omega) = \frac{\varepsilon''(\omega)}{\varepsilon'(\omega)^2 + \varepsilon''(\omega)^2}$$

By use of this equation, we change the representation of dielectric data from ε' and ε'' to M' and M'', respectively.

Figure 9 shows the variation of the real part of dielectric modulus (M') as a function of frequency over a range of temperature for all the composite films. At low frequencies and temperatures, M' tends to be very small but not approaching zero. As the temperature increases, however, the value of M' tends to zero at lower frequencies. This indicates that electrode polarization makes a significant contribution at lower temperatures and space charge accumulates at the interface. Moreover, a continuous increase in the value of M' has been observed with increasing frequency, with a tendency to level off at higher frequencies, in the usual sigmoidal manner, for all the temperatures. This observation may possibly be related to a lack of restoring force governing the mobility of charge carriers under the action of an induced electric field.[60] An increase in the value of M' with increasing frequency may be attributed to relaxation phenomena, because of the short-range mobility of charge carriers, which is spread over a range of frequencies.

Variation of the imaginary part of the dielectric modulus (M'') as a function of frequency at different temperatures is shown in Fig. 10. The variation of M'' with frequency at different temperatures gives useful information about the mechanism of charge transport, for example electrical transport and conductivity relaxation. At low temperatures (below 60°C), no peak was observed in this frequency range for all the samples under investigation. This may be

attributed to the greater relaxation time associated with the relaxation phenomenon at lower temperatures. At higher temperatures (above 60°C), however, the modulus plots are characterized by well defined asymmetric peaks at different frequencies. For all the samples, the plots obtained at high temperature are asymmetric relative to the peak maxima and the peaks are much broader than would be predicted by ideal Debye behavior. The broader nature of the peaks can be interpreted as the consequence of the distribution of relaxation time because of non-Debye-type relaxation behavior of the material. In the low-frequency region (to the left of the peaks) the charge carriers can be regarded as mobile over long distances and as performing successful hopping from one site to another. At higher frequencies (to the right of the peaks), however, the charge carrier motion is confined and only localized movement is observed. The frequency region in which the peak occurs is indicative of the transition from long-range to short-range mobility of the ions.[61] Moreover, the maximum of the peak frequency shifts toward higher frequencies with increasing temperature and with increasing BIT wt.%. The shifting of the peak suggests that the relaxation in which hopping of charge carriers may occur is thermally activated. This behavior also suggests that the relaxation time decreases with increasing temperature. It is found that the characteristic relaxation time (τ), calculated from the inverse of maximum frequency position, i.e. $(2\pi f_{max})^{-1}$, decreases from 10^{-3} to 10^{-5} with increasing temperature.

The temperature dependence of relaxation behavior can be interpreted by scaling of the modulus spectra. Figure 11 shows the normalized plot of M''/M''_{max} as a function of $\log f/f_{max}$ at different temperatures for pure PVDF film and for 10 wt.%-loaded BIT–PVDF composite film.

This graph, called the modulus master curve, provides insight into the dielectric phenomenon. The normalized plot shows that all the graphs for different temperature overlap on a single master curve with greater values of FWHM than the width of a typical Debye peak of 1.14 decades.[62] This behavior suggests that the relaxation process occurring at different frequencies is independent of temperature and has the same thermal energy. The non-symmetric behavior of normalized modulus plots is suggestive of stretched exponential character of relaxation times defined by the function:

$$\varphi(t) = \exp\left\{-\left(\frac{t}{\tau}\right)^{\beta}\right\}; (0<\beta<1) \qquad (9)$$

where $\varphi(t)$ is the relaxation of the electric field and β is a relaxation variable representative of the distribution of relaxation time.[63] The value of β varies in the range $(0<\beta<1)$. For an ideal Debye dielectric β is equal to unity and for non-Debye type relaxation behavior β is always less than unity. The value of β was determined from the full width at half maximum (FWHM) of the M'' plot as$(\beta = 1.14/FWHM)$. In this instance the value of β lies in the range 0.26–0.37 for all the samples. The low β value (i.e. higher FWHM) reveals the presence of non-Debye-type relaxation behavior. The values of FWHM, β, f_{max}, and τ at different temperatures for pure PVDF film and for 10 wt.% BIT–PVDF composite film are given in Table II.

CONCLUSIONS

We have shown that incorporation of BIT particles substantially affects the structural, morphological, and dielectric properties of these nanocomposite films. It is possible to prepare BIT–PVDF nanocomposites with the electroactive β and γ-phases of the polymer by spin coating. Incorporation of BIT particles increased the amounts of the electroactive β and γ phases of the polymer. The nanocomposite films had larger dielectric constants with relatively low dielectric loss. The effective dielectric constant calculated by use of the Maxwell–Garnet model was quite close to the experimental results for very low ceramic weight fractions. In addition, dielectric modulus plots confirmed non-Debye type relaxation behavior at high temperature. Our results indicate that the BIT–PVDF films are novel lead-free composite films which can be used in energy-storage devices.

ACKNOWLEDGEMENTS

The authors are grateful to the Analytical Instrumentation Research Facility, Jawaharlal Nehru University (AIRF JNU) New Delhi for TEM measurement.

REFERENCES

1. M. Arbatti, X. Shan, and Z. Cheng, *Adv. Mater.* 19, 1369 (2007).
2. Y. Rao and C.P. Wong, *J. Appl. Polym. Sci.* 92, 2228 (2004).
3. R.E. Newnham, *Annu. Rev. Mater. Sci.* 16, 47 (1986).
4. Z.M. Dang, Y. Shen, and C.W. Nan, *Appl. Phys. Lett.* 81, 4814 (2002).
5. Y. Bai, Z.-Y. Cheng, V. Bharti, H.S. Xu, and Q.M. Zhang, *Appl. Phys. Lett.* 76, 3804 (2000).
6. V. Tomer, G. Polizos, E. Manias, and C.A. Randall, *J. Appl. Phys.* 108, 074116 (2010).
7. R. Schroeder, L.A. Majewski, and M. Grell, *Adv. Mater.* 17, 1535 (2005).
8. M. Benz and W.B. Euler, *J. Appl. Polym. Sci.* 89, 1093 (2003).
9. R. Gregorio Jr, *J. Appl. Polym. Sci.* 100, 3272 (2006).
10. A.J. Lovinger, *Science* 220, 1115 (1983).
11. H.M.G. Correia and M.M.D. Ramos, *Comput. Mater. Sci.* 33, 224 (2005).
12. J. Scheinbeim, C. Nakafuku, B.A. Newman, and K.D. Pae, *J. Appl. Phys.* 50, 4399 (1979).
13. A.J. Lovinger, *Polymer* 22, 412 (1981).
14. J.S. Andrew and D.R. Clarke, *Langmuir* 24, 670 (2008).
15. A. Salimi and A.A. Yousefi, *Polym. Test.* 22, 699 (2003).
16. W. Ma, J. Zhang, and X. Wang, *J. Mater. Sci.* 43, 398 (2008).

17. J. Buckley, P. Cebe, D. Cherdack, J. Crawford, B. Seyhan Ince, M. Jenkins, J. Pan, M. Reveley, N. Washington, and N. Wolchover, *Polymer* 47, 2411 (2006).
18. D. Shah, P. Maiti, E. Gunn, D.F. Schmidt, D.D. Jiang, C.A. Batt, and E.P. Giannelis, *Adv. Mater.* 16, 1173 (2004).
19. J.S. Andrew and D.R. Clarke, *Langmuir* 24, 8435 (2008).
20. P. Martins, C.M. Costa, and S.L. Mendez, *Appl. Phys. A* 103, 233 (2011).
21. B.S.I. Gunduz, R. Alpern, D. Amare, J. Crawford, B. Dolan, S. Jones, R. Kobylarz, M. Reveley, and P. Cebe, *Polymer* 51, 1485 (2010).
22. S. Ramasundaram, S. Yoon, K.J. Kim, and C. Park, *Polym. Sci.* 46, 2173 (2008).
23. R. Singh, R.D.P. Sinha, and S. Chandra, *Ferroelectrics* 120, 293 (1991).
24. Z.D. Qing, W.D. Wei, Y. Jie, Z.Q. Liang, W.Z. Ying, and C.M. Sheng, *Chin. Phys. Lett.* 25, 4410 (2008).
25. C. Ehrhardt, C. Fettkenhauer, J. Glenneberg, W. Munchgesang, H.S. Leipner, M.D. Horst, S. Lemm, H. Beige, and S.G. Ebbinghaus, *J. Mater. Chem.* A2, 2266 (2014).
26. X. Huang, P. Jiang, and L. Xie, *Appl. Phys. Lett.* 95, 242901 (2009).
27. R.K. Goyal and A.B. Kulkarni, *J. Phys. D Appl. Phys.* 45, 465302 (2012).
28. G. Wang and A.C.S. Appl, *Mater. Interfaces* 2, 1290 (2010).
29. Y. Song, Y. Shen, H. Liu, Y. Lin, M. Li, and C.W. Nan, *J. Mater. Chem.* 22, 8063 (2012).
30. M.F. Lin, V.K. Thakur, E.J. Tanb, and P.S. Lee, *RSC Adv.* 1, 576 (2011).
31. P.C. Joshi, A. Mansingh, M.N. Kamalasanan, and S. Chandra, *Appl. Phys. Lett.* 59, 2389 (1991).
32. S.E. Cummins and L.E. Cross, *J. Appl. Phys.* 39, 2268 (1968).
33. A. Kumar and K.L. Yadav, *J. Alloys Compd.* 528, 16 (2012).
34. X.X. Wang, K.H. Lam, X.G. Tang, and H.L.W. Chan, *Solid State Commun.* 130, 695 (2004).
35. W.F. Sua, J.F. Lee, M.Y. Chen, and R.M. Ho, *J. Mater. Res.* 19, 2343 (2004).
36. H. Yang, Q. Ren, S. Guo, and G. Zhang, *Opt. Laser Tech.* 35, 291 (2005).
37. H. Yang, Q. Rena, G. Zhang, Y.T. Chow, H.P. Chan, and P.L. Chu, *Opt. Laser Tech.* 37, 259 (2005).
38. K. Han and T. Ko, *J. Alloys Compd.* 473, 490 (2009).
39. B.D. Stojanovic, C.O.P. Santos, M. Cilense, C. Jovalekic, and Z.Z. Lazarevic, *Mater. Res. Bull.* 43, 1743 (2008).
40. B.D. Cullity and S.R. Stock, *Elements of X-ray diffraction*, 3rd ed. (Upper Saddle River: Prentice Hall, 2001).
41. G.T. Davis, J.E. McKinney, M.G. Broadhurst, and S.C. Roth, *J. Appl. Phys.* 49, 4998 (1978).
42. M. Benz, W.B. Euler, and O.J. Gregory, *Langmuir* 17, 239 (2001).
43. T. Boccaccio, A. Bottino, G. Capannelli, and P. Piaggio, *J. Membr. Sci.* 210, 315 (2002).
44. A. Salimi and A.A. Yousefi, *Polym. Test.* 22, 699 (2003).
45. R. Gregorio and M. Cestari, *Polym. Sci.* 32, 859 (1994).
46. K. Tashiro, H. Kaito, and M. Kobayashi, *Polymer* 33, 14 (1992).
47. M.E. Mackay, A. Tuteja, P.M. Duxbury, C.J. Hawker, B.V. Horn, Z. Guan, G. Chen, and R.S. Krishnan, *Science* 311, 1740 (2006).
48. P. Martins, C. Caparros, R. Gonçalves, P.M. Martins, M. Benelmekki, G. Botelho, and S.L. Mendez, *J. Phys. Chem. C* 116, 15790 (2012).
49. A.C. Lopes, C.M. Costa, C.J. Tavares, I.C. Neves, and S. Lanceros-Mendez, *J. Phys. Chem. C* 115, 18076 (2011).
50. T.H. Young, D.J. Lin, J.J. Gau, W.Y. Chuang, and L.P. Cheng, *Polymer* 40, 5011 (1999).
51. H. Neumann and G. Arlt, *Ferroelectrics* 69, 179 (1986).
52. Z. Yua and C. Ang, *J. Appl. Phys.* 91, 794 (2002).
53. L. Yang, J. Qiu, H. Ji, K. Zhu, and J. Wang, *J. Mater. Sci.: Mater. Electron.* 25, 2126 (2014).
54. K. Yu, H. Wang, Y. Zhou, Y. Bai, and Y. Niu, *J. Appl. Phys.* 113, 034105 (2013).
55. J.C. Maxwell-Garnett, *Philos. Trans. R. Soc. Lond. A* 203, 385 (1904).
56. G. Subodh, C. Pavithran, P. Mohanan, and M.T. Sebastian, *J. Eur. Ceram. Soc.* 27, 3039 (2007).
57. T. Bhimasankaram, S.V. Suryanarayana, and G. Prasad, *Curr. Sci.* 74, 967 (1998).
58. Y. Kubouchi, Y. Kumetani, T. Yagi, T. Masusda, and A. Nakajima, *Pure Appl. Chem.* 61, 83 (1989).
59. I.M. Hodge, M.D. Ingram, and A.R. West, *J. Electroanal. Chem.* 74, 125 (1976).
60. M. Pant, D.K. Kanchan, and N. Gondaliya, *Mater. Chem. Phys.* 115, 98 (2009).
61. J. Liu, C.G. Duan, W.G. Yin, W.N. Mei, R.W. Smith, and J.R. Hardy, *J. Chem. Phys.* 119, 2812 (2003).
62. K. Lily, K. Kumari, and R.N.P.Choudhary Prasad, *J. Alloys Compd.* 453, 325 (2008).
63. P.S. Anantha and K. Hariharan, *Mater. Sci. Eng. B* 121, 12 (2005).